On the downshift of the class II Bragg resonance

Haiqi Fang, Lian Tang*, Pengzhi Lin*

State Key Laboratory of Hydraulics and Mountain River Engineering, Sichuan University, Chengdu 610065, China

*Corresponding author, E-mail address: tanglian@scu.edu.cn (L.Tang);

*Corresponding author, E-mail address: cvelinpz@scu.edu.cn (P. Lin)

ABSTRACT

In this paper, based on the multiple-scale expansion method, we derived a new closed-form solution for class II Bragg resonance. The proposed solution can accurately predict the reflection coefficient and effectively characterize the downshift behavior of the Bragg resonance. Subsequently, an analysis of the reflection's stationary point yields an exact formula that quantifies the magnitude of the wave frequency of resonance, and the accuracy of this formula are confirmed through comparisons against existing analytical and numerical solutions. Further investigation into the interactions between the waves and the ripples reveals the underlying mechanism of the downshift behavior, which highlights the significant influence of wave re-reflection by the doubly sinusoidal ripples. In particular, the process in which waves are initially reflected by one of the ripple components and subsequently re-interacts with the corresponding conjugate component, results in the downward shift from the Bragg resonance condition. Moreover, the study of the effect of ripple length on Bragg resonance revealed that the downshift magnitude increases up to a certain limit as the ripple length tends to infinity, and this limit is substantially affected by the ripple amplitudes. In addition, the effects of the two ripple components are studied, which reveals the existence of a threshold ratio of the second to the first ripple wavenumber for a specific water depth. When the ratio is smaller than the threshold value, the downshift behavior of Bragg resonance is primarily influenced by the first ripple component. Conversely, as the ratio exceeds this value, it transits into the the situation where the downshift behavior is dominated by the second ripple component.

KEYWORDS

Class-II Bragg resonance

Analytical solution for wave reflection

Theoretical formula for downshift

i. Introduction

Bragg resonance, known as normally incident waves being strongly reflected by sinusoidal ripples, exhibits maximum reflection when the wavelength of the incident wave is two times the wavelength of the sinusoidal ripple undulations. Davies and Heathershaw (1984) pioneered the study in a laboratory framework, where the phenomenon was first discovered, followed by further experimental studies (Magne et al., 2005; Peng et al., 2019) and analytical studies (Fang et al., 2023; Liu et al., 2019; Mei, 1985). Bragg resonance has been demonstrated to play a vital role in coastal processes, as it protects shoreline buildings and prevents soil erosion by reflecting a substantial portion of the wave energy, and this concept leads to the development of artificial bars for coastal protection (Kirby and Anton, 1990; Liu et al., 2015).

In practice, bottom ripples often exhibit complex shapes rather than being strictly sinusoidal-shaped. Notably, the ripples composed of two sinusoids with different wavenumbers K_1 and K_2 $(K_2 > K_1)$, namely, doubly sinusoidal ripples, can interact with the incident waves and generate higher-order reflections, specifically referred to as class II Bragg resonance. Experimental investigation conducted by Guazzelli et al. (1992) first confirmed four resonant conditions for the incident wave number $\tilde{k}$: $\tilde{k} = (K_2 - K_1)/2$ (for class II sub-harmonic resonance), $\tilde{k} = (K_1 + K_2)/2$ (for class II super-harmonic resonance), $\tilde{k} = K_1/2$ and $\tilde{k} = K_2/2$ (for class I resonance), where the class II Bragg resonance will occur by satisfying either the first two resonant conditions. In particular, the reflection induced by sub-harmonic resonance was found to be significantly stronger, even though bottom undulations are small (Belzons et al., 1991; Guazzelli et al., 1992).

Moreover, numerous studies have been conducted on class II sub-harmonic Bragg resonance, providing profound insights into this phenomenon. Guazzelli et al. (1992) developed a wide-spacing approximation by subdividing ripples into smaller subsystems of steps, and their findings highlighted the significant contribution of evanescent modes in intensifying resonant reflection. In addtion, Seo (2014) developed a numerical method with higher computational efficiency and accuracy, where the significant effect of the ripple length on the reflection coefficient was emphasized. Recently, Xu et al. (2023) employed the Homotopy analysis

method to examine the energy characteristics for wave scattering of class II Bragg resonance, revealing the underlying influence of the ripple wavenumbers and amplitudes on energy distribution.

Notably, the numerical study of the high-order spectral method (Liu and Yue, 1998) highlighted a noticeable downward shift of the incident wavenumber from the resonance condition $(k < (K_2 - K_1)/2)$. Notably, the downshift behavior is not only occurred in class II resonance problem, but also has been observed in wave scattering across diverse topographical configurations. In particular, Liang et al. (2020) and Peng et al. (2022) fully investigate the downshift behavior induced by sinusoidal ripples conducted comprehensive analyzes of the downshift behavior induced by sinusoidal ripples, and proposed theoretical formulas to quantify the downshift magnitude. Furthermore, Liu (2023) derived mathematical expressions characterizing the downshift of resonance wavenumber for waves scattering by five different types of artificial bars. Studying the downshift behavior of Bragg resonance holds notable significance, as it provides essential parameters for the design of artificial bars and enables optimization of the cross-sectional shape and arrangement of the Bragg breakwater. Although extensive research has been conducted on downshift phenomenon, it is important to note that, to the best of the authors' knowledge, a theoretical investigation into the downshift of class II Bragg resonance has not yet been proposed, and the underlying mechanism behind its formation remains elusive. Thus, it is necessary to establish a theoretical formula that quantifies its magnitude, which can facilitate a comprehensive exploration of the factors influencing this downward shift behavior.

The multiple-scale expansion method, as an ideal tool for investigating wave scattering in the vicinity of resonance, has found extensive application in Bragg resonance studies. Mei (1985) pioneered the process and developed analytical solutions to analyze wave scattering induced by sinusoidal ripples. Subsequently, the method and solutions of Mei (1985) was extended to study oblique incidence (Kirby, 1993; Mei et al., 1988), irregular bottom conditions under random waves (Ardhuin and Herbers, 2002), and the inclusion of current effects (Ardhuin and Magne, 2007; Kirby, 1988). Remarkably, Rey et al. (1996) studied class II Bragg resonance and derived analytical solutions for wave reflection and transmission, thereby providing theoretical understanding of this phenomenon. However, the theory of Rey et al. (1996) predicts

that the maximum reflection occurs at the resonance condition, which cannot descibe the downshift behavior of class II Bragg resonance, and we will demonstrate that this arises from the ignorance of certain wave-ripple interactions in their derivation, i.e., $\tilde{k} \pm K_1 \mp K_1$ and $\tilde{k} \pm K_2 \mp K_2$. Consequently, by accounting for all the relevant wave-ripple interaction in this problem, a new analytical solution can be derived to enable capable of prediction of the downshift behavior.

In this paper, based on the multiple-scale expansion method, we study the class II sub-harmonic Bragg resonance, especially the downshift behavior that occurs in this process. In section ii, we present the derivation of the analytical solutions for wave reflection, and based on which, a mathematical formula that quantifies the magnitude of the wave frequency downshift is proposed. In section iii, we verify the present theory by comparing with numerical solutions calculated based on the method in Seo (2014), and we discuss the effects of ripple amplitude, ripple length and the two ripple components on the downshift magnutide. In section iv, the main results and conclusions are outlined.

ii. Mathematical derivation

This section studies the propagation of waves over doubly periodic sinusoidal ripples based on the multiple-scale expansion method. As depicted in Fig. 1, the ripples are fixed at an average water depth of h below the mean water level, and δ denotes the function of the ripple undulations

$$\delta = \frac{-i}{2} D_1 e^{iK_1 x} + \frac{i}{2} D_2 e^{-iK_2 x} + \text{C. C.}, \tag{1}$$

in which K_1 and K_2 $(K_1 < K_2)$ represent the wavenumbers the two components of the ripples. In this paper, the symbol 'C.C.' denotes the conjugate component, and i stands for the unit imaginary number. D_1, D_2 are the ripple amplitudes, characterized by the small parameter ε. The incident wave is assumed to be periodic in both time and space, with ω and k representing its frequency and wavenumber, which is allowed to slowly modulate in both temporal and spatial scales during wave transformation.

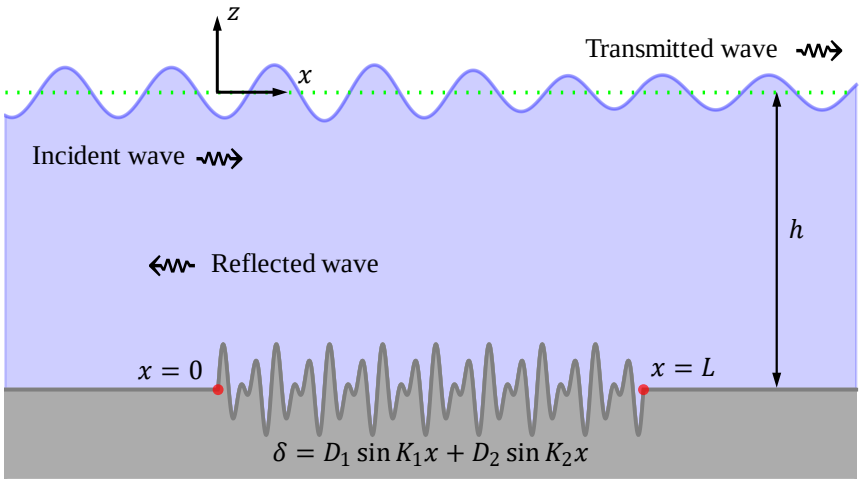

Fig. 1 Schematic of the wave propagation domain.

We assume the fluid to be inviscid and incompressible and the flow is irrotational. A train of infinitesimal waves is incident over a series of doubly sinusoidal ripples positioned at $[0, L]$, where wave scattering occurs, generating reflected and transmitted waves. Here, denote ϕ as the velocity potential function, which satisfies the surface linearized Laplace equation in the fluid domain,

$$\frac{\partial^2 \phi}{\partial x^2} + \frac{\partial^2 \phi}{\partial z^2} = 0 \ (-h + \delta < z < 0). \tag{2}$$

On the free surface, the linearized kinematic and dynamic boundary conditions can be combined to give

$$\frac{\partial^2 \phi}{\partial t^2} + g \frac{\partial \phi}{\partial z} = 0 \ (z = 0), \tag{3}$$

in which g is the gravitational acceleration. At the bottom, the no-flux boundary condition can be expanded into Taylor series form

$$\frac{\partial \phi}{\partial z} = \frac{\partial}{\partial x}\left(\delta \frac{\partial \phi}{\partial x}\right) + \frac{\partial}{\partial x}\left(\frac{\delta^2}{2} \frac{\partial^2 \phi}{\partial x^2}\right) + \cdots \ (z = -h). \tag{4}$$

A. Multiple-scale expansion analysis

We consider wave reflection in the vicinity of the sub-harmonic resonance, and the wavenumber $\tilde{k}$ that satisfies the sub-harmonic resonance condition is introduced

$$\tilde{k} = \frac{1}{2}(K_2 - K_1). \tag{5}$$

Following the method of Rey et al. (1996), we introduce the slow variables up to the second-order, $\xi_1 = \varepsilon x, \xi_2 = \varepsilon^2 x, \tau_1 = \varepsilon t, \tau_2 = \varepsilon^2 t$, and the multiple-scale expansion up to third-order

$$\phi = \varepsilon \phi_1 + \varepsilon^2 \phi_2 + \varepsilon^3 \phi_3 + O(\varepsilon^4). \tag{6}$$

in which $\phi_1 = \phi_1(x, z, t, \xi_1, \tau_1, \xi_2, \tau_2)$, etc. $O(\,)$ is an infinitesimal quantity of the same order.

By substituting Eq. (6) into the governing equation Eq. (2) and the boundary conditions Eqs. (3) and (4), boundary value problems (BVPs) can be obtained for each order of ε upon the separation of different orders.

The first-order problem

The first-order problem is homogeneous for ϕ, and the solution can be expressed as

$$\phi_1 = \psi^+ e^{i(\tilde{k}x - \tilde{\omega}t)} + \psi^- e^{i(-\tilde{k}x - \tilde{\omega}t)} + \text{C. C.}, \tag{7}$$

in which $\tilde{\omega}$ is the angular frequency, satisfying the dispersion equation, $\tilde{\omega} = g\tilde{k}\tanh\tilde{k}h$, and the wave frequency is defined as $\tilde{f} = \tilde{\omega}/(2\pi)$. The superscripts $+$ and $-$ refer to the incident and reflected waves, respectively. ψ^+ and $\psi^-$are the vertical profiles

$$\psi^{\pm} = -\frac{ig}{2\tilde{\omega}}\frac{\cosh\tilde{k}(z+h)}{\cosh\tilde{k}h}A^{\pm} \tag{8}$$

in which $A^{\pm}$ are the complex wave amplitudes, which are governed by the slow variables, $A^{\pm} = A^{\pm}(\xi_1, \tau_1, \xi_2, \tau_2)$.

The second-order problem

Substituting the solution of ϕ_1 (Eq. (7)) into the second-order problem, the solution of ϕ_2 can be proposed

$$\begin{aligned}\phi_2 = {} & \beta^+ e^{i(\tilde{k}x - \tilde{\omega}t)} + \beta^- e^{i(-\tilde{k}x - \tilde{\omega}t)} + \beta_1^+ e^{i[(\tilde{k}+K_1)x - \tilde{\omega}t]} + \beta_1^- e^{i[-(\tilde{k}+K_1)x - \tilde{\omega}t]} \\ & + \beta_{-1}^+ e^{i[(\tilde{k}-K_1)x - \tilde{\omega}t]} + \beta_{-1}^- e^{i[-(\tilde{k}-K_1)x - \tilde{\omega}t]} + \beta_2^+ e^{i[(\tilde{k}+K_2)x - \tilde{\omega}t]} \\ & + \beta_2^- e^{i[-(\tilde{k}+K_2)x - \tilde{\omega}t]} + \beta_{-2}^+ e^{i[(\tilde{k}-K_2)x - \tilde{\omega}t]} + \beta_{-2}^- e^{i[-(\tilde{k}-K_2)x - \tilde{\omega}t]} + \text{C. C.},\end{aligned} \tag{9}$$

in which $\beta_j^{\pm}$ and $\beta_{-j}^{\pm}$, where $j = 1, 2$, can be solved from the inhomogeneous problems

$$\beta_j^{\pm} = \pm\frac{g\tilde{k}D_jA^{\pm}}{4\tilde{\omega}\cosh\tilde{k}h}\frac{\tilde{\omega}^2\sinh(\tilde{k}+K_j)z + g(\tilde{k}+K_j)\cosh(\tilde{k}+K_j)z}{\tilde{\omega}^2\cosh(\tilde{k}+K_j)h - g(\tilde{k}+K_j)\sinh(\tilde{k}+K_j)h}, \tag{10}$$

and

$$\beta_{-j}^{\pm} = \mp\frac{g\tilde{k}D_jA^{\pm}}{4\tilde{\omega}\cosh\tilde{k}h}\frac{\tilde{\omega}^2\sinh(\tilde{k}-K_j)z + g(\tilde{k}-K_j)\cosh(\tilde{k}-K_j)z}{\tilde{\omega}^2\cosh(\tilde{k}-K_j)h - g(\tilde{k}-K_j)\sinh(\tilde{k}-K_j)h}. \tag{11}$$

Based on the Fredholm's Alternative Theorem (Friedman, 1956), the first set of solvability conditions can be obtained

$$\frac{\partial A^{\pm}}{\partial\tau_1} \pm C_g\frac{\partial A^{\pm}}{\partial\xi_1} = 0, \tag{12}$$

in which C_g is the group velocity, with $C_g = \tilde{\omega}(1 + 2\tilde{k}h\,\text{csch}\,2\tilde{k}h)/(2\tilde{k})$. Once Eq. (12) is

satisfied, the coefficients $\beta^{\pm}$ can be solved to give

$$\beta^{\pm} = \mp \frac{g(z+h)\sinh \tilde{k}(z+h)}{2\tilde{\omega}\cosh \tilde{k}h} \frac{\partial A^{\pm}}{\partial \xi_1}. \tag{13}$$

The third-order problem

For the third-order problem, the resonant wave modes, $e^{i(\tilde{k}x-\tilde{\omega}t)}$ and $e^{i(-\tilde{k}x-\tilde{\omega}t)}$ are considered. The other harmonics, which have not related to resonance, are ignored. And ϕ_3 can be expressed as

$$\phi_3 = \left[\gamma^{+} e^{i(\tilde{k}x-\tilde{\omega}t)} + \gamma^{-} e^{i(-\tilde{k}x-\tilde{\omega}t)} + \text{C. C.}\right] + \text{NRT}, \tag{14}$$

in which $\gamma^{\pm}$ are the vertical profiles to be determined and 'NRT' denotes the non-resonant terms. Solvability of $\gamma^{\pm}$ can be ensured by the governing equation

$$\left(\frac{d^2}{dz^2} - \tilde{k}^2\right)\gamma^{\pm} = \frac{g\,\mathrm{sech}\,\tilde{k}h}{2\tilde{\omega}}\left[\left(\mp 2\tilde{k}\frac{\partial A^{\pm}}{\partial \xi_2} + i\frac{\partial^2 A^{\pm}}{\partial \xi_1^2}\right)\cosh \tilde{k}(z+h) + 2i\tilde{k}(z+h)\sinh \tilde{k}(z+h)\frac{\partial^2 A^{\pm}}{\partial \xi_1^2}\right] \tag{15}$$

and boundary conditions

$$\left(g\frac{d\gamma^{\pm}}{dz} - \tilde{\omega}^2\gamma^{\pm}\right)\Big|_{z=0} = g\frac{\partial A^{\pm}}{\partial \tau_2} + \frac{ig}{2\tilde{\omega}}\frac{\partial^2 A^{\pm}}{\partial \tau_1^2} \mp \frac{ih\tilde{\omega}^2}{k}\frac{\partial^2 A^{\pm}}{\partial \xi_1 \partial \tau_1} \tag{16}$$

and

$$\begin{aligned}\left.\frac{d\gamma^{\pm}}{dz}\right|_{z=-h} &= \frac{\partial}{\partial x}\left(\delta\frac{\partial \phi_2}{\partial x}\right) \\ &= \pm\frac{i\tilde{k}}{2}\left[D_2(\tilde{k}+K_1)\beta_1^{\mp} - D_1(\tilde{k}-K_2)\beta_{-2}^{\mp}\right]\Big|_{z=-h} \\ \pm\frac{i\tilde{k}}{2}&\left[-D_1(\tilde{k}-K_1)\beta_{-1}^{\pm} + D_2(\tilde{k}+K_2)\beta_2^{\pm} + D_1(\tilde{k}+K_1)\beta_1^{\pm} - D_2(\tilde{k}-K_2)\beta_{-2}^{\pm}\right]\Big|_{z=-h}\end{aligned} \tag{17}$$

where the terms on the right side of Eq. (17) stands for the effect of the wave-ripple-ripple interactions, as illustrated in Fig. 2.

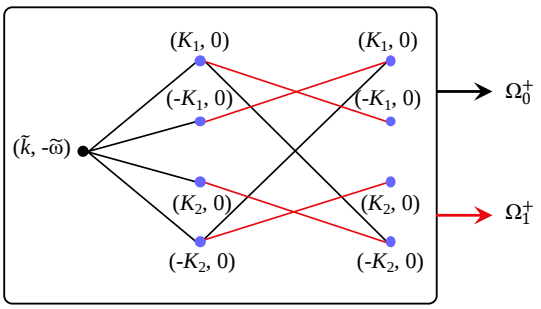

Fig. 2 Illustration of the wave-ripple-ripple interactions.

In Fig. 2, the black lines refer to the interactions: $\tilde{k}+K_1-K_2\rightarrow-\tilde{k}$ and $\tilde{k}-K_2+K_1\rightarrow-\tilde{k}$, which represents that the incident wave is initially reflected by one ripple component and then interacts with the other ripple component, thereby intensifying the reflected wave mode. And this process leads to the first term on the right side of Eq. (17) stands for the effect of the wave-ripple interactions considered in the analysis of Rey et al. (1996):

$$\beta_1^{\mp}e^{i[\mp(\tilde{k}+K_1)x-\tilde{\omega}t]}\oplus\frac{\mp i}{2}D_2e^{\pm iK_2x},\quad \beta_{-2}^{-}e^{i[\mp(\tilde{k}-K_2)x-\tilde{\omega}t]}\oplus\frac{\pm i}{2}D_1e^{\mp iK_1x}, \tag{18}$$

in which the symbol $\oplus$ represents the interactions between the wave modes and ripple components.

However, the second term on the right side of Eq. (17) represents the effects of the conjugate component of the ripples on waves modes, as highlighted in Fig. 2, which was ignored by Rey et al. (1996), represented by the following interactions

$$\begin{aligned}&\beta_1^{\pm}e^{i[\pm(\tilde{k}+K_1)x-\tilde{\omega}t]}\oplus\frac{\pm i}{2}D_1e^{\mp iK_1x},\quad \beta_{-2}^{\pm}e^{i[\pm(\tilde{k}-K_2)x-\tilde{\omega}t]}\oplus\frac{\mp i}{2}D_2e^{\pm iK_2x}\\&\beta_{-1}^{\pm}e^{i[\pm(\tilde{k}-K_1)x-\tilde{\omega}t]}\oplus\frac{\mp i}{2}D_1e^{\pm iK_1x},\quad \beta_{2}^{\pm}e^{i[\pm(\tilde{k}+K_2)x-\tilde{\omega}t]}\oplus\frac{\pm i}{2}D_2e^{\mp iK_2x},\end{aligned} \tag{19}$$

which are characterized by the process: $\tilde{k}\pm K_1\mp K_1\rightarrow\tilde{k}$ and $\tilde{k}\pm K_2\mp K_2\rightarrow\tilde{k}$, which represents the interactions: wave-ripple component-conjugate ripple component, where the incident wave is first reflected by one ripple component and subsequently re-reflected by the conjugate of the ripple component, resulting in an intensified incident wave mode.

By employing the Fredholm's Alternative Theorem (Friedman, 1956) to Eqs. (15)-(17), the second solvability conditions can be obtained

$$\frac{\partial A^{\pm}}{\partial\tau_2}\pm C_g\frac{\partial A^{\pm}}{\partial\xi_2}+i\alpha^{\pm}\frac{\partial^2A^{\pm}}{\partial{\xi_1}^2}+i\Omega_0^{\pm}\frac{\partial A^{\mp}}{\partial\tau_1}+i\Omega_1^{\pm}A^{\pm}=0, \tag{20}$$

where

$$\alpha^{\pm}=\frac{1+8\tilde{k}^2h^2-\cosh4\tilde{k}h+8\tilde{k}h\left(\sinh2\tilde{k}h-2\tilde{k}h\cosh2\tilde{k}h\right)}{4\tilde{\omega}\left(2\tilde{k}h+\sinh2\tilde{k}h\right)^2}, \tag{21}$$

$$\Omega_0^{\pm}=-\frac{D_1D_2\tilde{k}\tilde{\omega}(K_1+K_2)}{4\sinh2\tilde{k}h}\frac{g\left(\tilde{k}+K_1\right)-\tilde{\omega}^2\tanh\left(\tilde{k}+K_1\right)h}{\tilde{\omega}^2-g\left(\tilde{k}+K_1\right)\tanh\left(\tilde{k}+K_1\right)h}, \tag{22}$$

As can be seen in Fig. 2, $\Omega_0^{\pm}$ is generated during the process described with black arrow, and $\Omega_1^{\pm}$ is induced by the path highlighted by the red arrow, which can be expressed as

$$\Omega_1^{\pm}=\sum_{j=1}^{2}\sigma_j\,D_j^2, \tag{23}$$

in which

$$\sigma_j = -\frac{S_j \tilde{k}\tilde{\omega}\,\mathrm{csch}\,2\tilde{k}h}{4\mathcal{F}(\tilde{k}-K_j)\mathcal{F}(\tilde{k}+K_j)}, \tag{24}$$

where $\mathcal{F}(l)$ is a function on the variable l,

$$\mathcal{F}(l) = \tilde{\omega}^2 \cosh lh - gl \sinh lh\,, \tag{25}$$

and S_j $(j = 1, 2)$ is defined as

$$S_j = -2g\tilde{\omega}^2\left(\tilde{k}^2 \cosh 2\tilde{k}h + K_j^2 \cosh 2K_j h\right) + K_j\left[\tilde{\omega}^4 - g^2\left(\tilde{k}^2 - K_j^2\right)\right]\sinh 2K_j h\,. \tag{26}$$

We introduce transforms of temporal and spatial scales to recover x and t, with $\varepsilon\partial/\partial\tau_1 + \varepsilon^2\partial/\partial\tau_2 \to \partial/\partial t$ and $\varepsilon\partial/\partial\xi_1 + \varepsilon^2/\partial\xi_2 \to \partial/\partial x$, which enables $A^{\pm}(\xi_1, \tau_1, \xi_2, \tau_2)$ to return to $A^{\pm}(x, t)$. Thus, Eq. (20) combined the first solvability conditions Eq. (12), gives the evolution equations coupling the amplitudes of the first-order incident and reflected waves,

$$\overbrace{\frac{\partial A^+}{\partial t} + C_g\frac{\partial A^+}{\partial x} + i\alpha^+\frac{\partial^2 A^+}{\partial x^2} + i\Omega_0^+\frac{\partial A^-}{\partial t}}^{\text{Identical to Rey et al.(1996)}} + i\Omega_1^+ A^+ = 0, \tag{27}$$

and

$$\overbrace{\frac{\partial A^-}{\partial t} - C_g\frac{\partial A^-}{\partial x} + i\alpha^-\frac{\partial^2 A^-}{\partial x^2} + i\Omega_0^-\frac{\partial A^+}{\partial t}}^{\text{Identical to Rey et al.(1996)}} + i\Omega_1^- A^- = 0, \tag{28}$$

in which the first four terms are identical the evolution equations proposed by Rey et al. (1996), with $\alpha^{\pm}$ and $\Omega_0^{\pm}$ representing the dispersion effect and the wave-ripple interactions described in Eq. (18). However, compared to the theory of Rey et al. (1996), an additional term is presented on the left hand side of Eqs. (27) and (28), arising from the interactions among the wave, the ripple component and the conjugate ripple component, which is detailed in Eq. (19).

B. Analytical solution for wave scattering

As illustrated in Fig. 1, a train of incident waves, with a small amplitude A_0 $(A_0 \ll 1)$, both temporally and spatially periodic arrive from $x = -\infty$, which are continuously reflected by the doubly sinusoidal ripples (located at $0 < x < L$, and L denotes the total length of the ripples with $kL \gg 1$), forming reflected waves that propagate in the opposite direction and produce standing waves by the superposition of the incident and reflected waves. In the region $x > L$, where the varying bottom vanishes, only the forward propagating mode exists, designated as transmitted waves.

Let the waves be slightly detuned from the class II Bragg resonance, and wave frequencies are $\omega = \tilde{\omega} + \omega'$, implying wavenumber detuning $k = \tilde{k} + k'$. $A^{\pm}$ can be expressed as

$$A^{+} = A_0 T(x) e^{ik'x - i\omega' t}, \quad A^{-} = A_0 R(x) e^{-ik'x - i\omega' t}. \tag{29}$$

In the incidence $(x < 0)$ and transmission zones $(x > L)$ without ripples, the evolution equations are homogeneous, leading to the boundary conditions for $T(x)$ and $R(x)$

$$T(0) = 1, \quad R(L) = 0. \tag{30}$$

At $0 < x < L$, by substituting Eq. (29) into Eqs. (27) and (28), a linear system of equations can be obtained

$$\begin{aligned} i\Omega_0^{+} R(x) + [-i\omega' + i\alpha^{+}(\omega')^2 + i\Omega_1^{+}]T(x) + C_g \frac{dT(x)}{dx} = 0, \\ i\Omega_0^{-} T(x) + [-i\omega' + i\alpha^{-}(\omega')^2 + i\Omega_1^{-}]R(x) - C_g \frac{dR(x)}{dx} = 0, \end{aligned} \tag{31}$$

Similar to the solving procedure presented in Mei (1985) and Rey et al. (1996), the linear system (Eq. (31)) combined with boundary conditions (Eq. (30)) can be solved to give

$$\begin{aligned} R(x) &= \frac{-Q_1 \sin P(L-x)}{iP\cos PL + Q_2 \sin PL}, \\ T(x) &= \frac{iP\cos P(L-x) + Q_2 \sin P(L-x)}{iP\cos PL + Q_2 \sin PL}, \end{aligned} \tag{32}$$

in which Q_1 and Q_2 are real parameters, defined as

$$Q_1 = -\frac{\Omega_0^{+}}{C_g}, \tag{33}$$

and

$$Q_2 = \frac{\omega' - \alpha^{+}(\omega')^2}{C_g} - \frac{\Omega_1^{+}}{C_g}. \tag{34}$$

P is a complex, defined as

$$P = \sqrt{\frac{[\omega' - \alpha^{+}(\omega')^2 - \Omega_1^{+}]^2 - (\Omega_0^{+})^2}{C_g^2}}. \tag{35}$$

And the solution of reflection rate $\tilde{R} = |R(0)|$ can be derived

$$\tilde{R} = \sqrt{\frac{Q_1^2}{Q_2^2 + P^2 \cot^2 PL}}, \tag{36}$$

It is evident that the only difference between the present solution Eq. (36) and the solution of Rey et al. (1996) lies in the terms Q_2 and P. If Ω_1^{+} is set to zero, the present solution reduces to their solution,

$$\tilde{R}^{\mathrm{R}} = \sqrt{\frac{\left(Q_1^{\mathrm{R}}\right)^2}{\left(Q_2^{\mathrm{R}}\right)^2 + (P^{\mathrm{R}})^2 \cot^2 P^{\mathrm{R}} L}} \tag{37}$$

in which the superscript 'R' represents the results of Rey et al. (1996) and

$$\begin{aligned} Q_1^{\mathrm{R}} &= -\frac{\Omega_0^+}{C_g^+} \\ Q_2^{\mathrm{R}} &= \frac{\omega' - \alpha^+(\omega')^2}{C_g} \\ P^{\mathrm{R}} &= \sqrt{\frac{[\omega' - \alpha^+(\omega')^2]^2 - (\Omega_0^+)^2}{C_g^2}} \end{aligned} \tag{38}$$

C. Derivation of the solution for downshift

In this subsection, a theoretical expression of the downshift magnitude of the wave frequency is presented. The solution of reflection coefficient, denoted as $\tilde{R}^{\mathrm{TP}} = \tilde{R}^{\mathrm{TP}}(\omega')$, is expressed in Eq. (36). The wave frequency shift at maximum reflection, denoted as f_{shift}, can be obtained from the derivative of the squared reflection coefficient with respect to ω' being equal to zero. At $\omega' = 2\pi f_{\mathrm{shift}}$

$$\frac{\partial}{\partial \omega'}\left(\frac{Q_1^2}{Q_2^2 + P^2 \cot^2 PL}\right) = 0. \tag{39}$$

And Eq. (39) is equivalent to

$$\frac{\partial Q_1}{\partial \omega'}\left(Q_2^2 + P^2 \cot^2 PL\right) - Q_1\left(Q_2 \frac{\partial Q_2}{\partial \omega'} + P \cot PL \frac{\partial P \cot PL}{\partial \omega'}\right) = 0, \tag{40}$$

which, combined with Eqs. (33)-(35), gives

$$\frac{\Omega_0^+(1 - ML \coth ML)}{C_g^3 \sinh ML}(1 - 2\alpha^+\omega')[\alpha^+(\omega')^2 - \omega' + \Omega_1^+] = 0, \tag{41}$$

where $M = -iP$. The left hand side of Eq. (41) is the product of multiple factorizations, which are not-related to the resonance except for the last term. Thus, one of the roots of the quadratic polynomial $\alpha^+(\omega')^2 - \omega' + \Omega_1^+$ corresponds to the solution of f_{shift}, and this gives

$$f_{\mathrm{shift}} = \frac{1 - \sqrt{1 - 4\alpha^+\Omega_1^+}}{4\pi\alpha^+} = \frac{1 - \sqrt{1 - 4\alpha^+(\sigma_1 D_1^2 + \sigma_2 D_2^2)}}{4\pi\alpha^+}, \tag{42}$$

which is exact solution of the magnitude of the wave frequency downshift. Denote f_{res} as the resonance frequency, which can be expressed as

$$f_{\text{res}} = \tilde{f} + f_{\text{shift}} = \tilde{f} + \frac{1 - \sqrt{1 - 4\alpha^{+}(\sigma_1 D_1^2 + \sigma_2 D_2^2)}}{4\pi\alpha^{+}}, \tag{43}$$

and the resonance frequency of Rey et al. (1996) can be expressed as

$$f_{\text{res}}^{R} = \tilde{f}. \tag{44}$$

It is clear that the process, wave-ripple component-conjugate ripple component, is of significant importance in inducing the downshift behavior. In the analysis of Rey et al. (1996), this interaction process is ignored, and the numerator of Eq. (42) reduces to 0, leading to $f_{\text{shift}} = 0$ and thereby failing to predict the downward shift of wave frequency.

iii. Results and analysis

A. Comparisons and verification

The present analytical solution of reflection coefficient, Eq. (36), is compared with the analytical solution of Rey et al. (1996) in Eq. (37). In addition, to further validate the theoretical formula that quantifies the downshift magnitude of the wave frequency of class II Bragg resonance in Eq. (43), we employed the Eigenfunction expansion method in Seo (2014) to calculate numerical results to provide additional verification, where the ripples is discretized into a series of narrow shelves, and the problem is simplified as the propagation of waves with evanescent modes over a succession of domains of constant depth separated by small steps.

During the process of the calculation based on the method Seo (2014), two numerical schemes are empolyed to verify the convergence of the numerical solution: scheme A considers 50 equally spaced steps per single ripple period length L_0 and 3 evanescent modes, and scheme B includes 100 steps per single ripple period length L_0 and 4 evanescent modes.

The geometrical configuration is following the set-up of an experiment of Guazzelli et al. (1992), with $h = 2.5$ cm, $L_0 = 48$ cm, $K_1 = \pi/3$ cm^{-1}, $K_2 = \pi/2$ cm^{-1} and $\tilde{k} = \pi/12$ cm^{-1}, except for the ripple length L, which is fixed at 1.44 m, to ensure the assumption $kL \gg 1$. In this example, let the bottom amplitudes of the two components be equal, represented by $D = D_1 = D_2$. Numerous bottom amplitudes are adopted to examine the validity of the present solution, with D/h =0.15, 0.20, respectively.

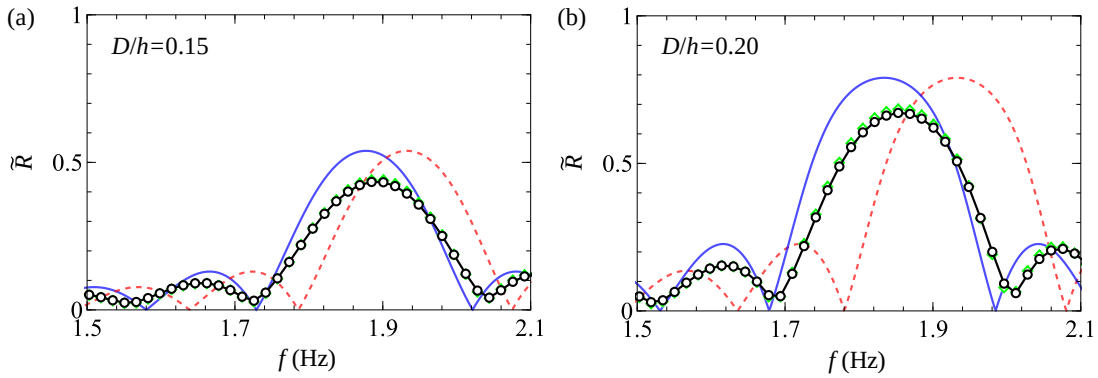

Fig. 3 Comparison of the reflection coefficient among the present solution (blue solid line, Eq. (36)), analytical solution from Rey et al. (1996) (red dashed line, Eq. (37)), numerical solutions calculated based on the method of Seo (2014) with Scheme A (green diamond) and Scheme B (black dot), for varying ripple amplitude D. (a) D/h = 0.15; (b) D/h = 0.20.

Fig. 3 presents the analytical and numerical solutions of reflection coefficients under two bottom amplitude conditions, namely, D/h = 0.15 and 0.20. The numerical results calculated based on the two sets of schemes agree with each other, thus ensuring the convergency of the computation by using Scheme A or Scheme B. Overall agreements between the present solution and numerical calculations can be seen in these cases. In addition, a noticable downshift of the wave frequency of the maximum reflection can be observed, which can be well captured by the present solution, and the corresponding wave frequency f_{res} compares with that of numerical solutions, which is more obvious as the ripples become steeper. Moreover, to further quantify the influence of bottom amplitude on the downwards shift, the results of f_{res} versus D/h are illustrated in Fig. 4.

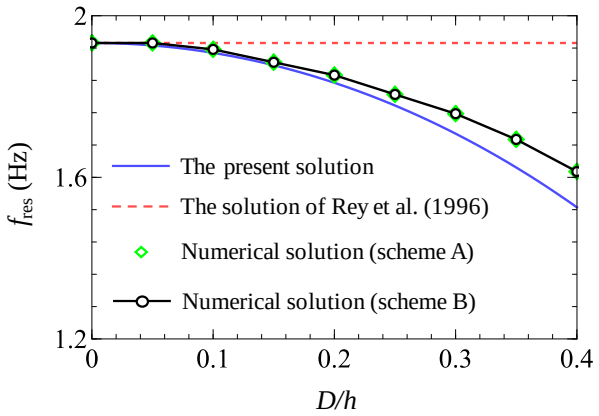

Fig. 4 Comparison of the wave frequency of resonance predicted by the present theoretical formula (blue solid line, Eq. (43)), theory of Rey et al. (1996) (red dashed line, Eq. (44)),

numerical solutions calculated based on the method of Seo (2014) with Scheme A (green diamond) and Scheme B (black dot), for varying *D/h*.

Fig. 4 presents the significant impact of the bottom amplitude on the wave frequency of class II Bragg resonance, in which a noticeable downward shift of resonant frequency is observed with the increase of *D/h*. Both the theoretical formula Eq. (43) and numerical solutions show an approximate parabolic downward trend, and satisfactory agreements are obtained for *D/h*<0.15, where $f_{\mathrm{res}} \approx \tilde{f} + (\sigma_1 + \sigma_2)D^2/(2\pi)$ for small *D/h*, which is a standard parabolic function. However, with the increase of bottom amplitude, slight differences between the numerical and theoretical results are presented, this is because the multiple-scale expansion used in the present analysis is restricted to the third-order accuracy of ε, and a better result can be hopefully obtained if a higher-order expansion is applied.

B. The ripple length effect on the resonance

It has been demonstrated that, for wave scattering problems, the increase of the length of the ripples L can significantly enhance wave reflection and change the magnitude of the frequency downshift (Liu, 2023; Liu et al., 2019; Peng et al., 2022; Rey et al., 1996). Moreover, based on the geometric configuration of artificial-bar types, Liu (2023) further revealed the principle of the frequency downshift varying with the length of the topography, as L tends to infinity, the magnitude of the downward shift converges to a limitation.

To further study the variations of the reflection coefficient and the resonance frequency downshift behavior due to the change of ripple length L. We follow the geometric configuration employed in the last section, where $D/h = 0.2$, with the length of the ripples L varying, to calculate the reflection coefficient as wave frequency varies.

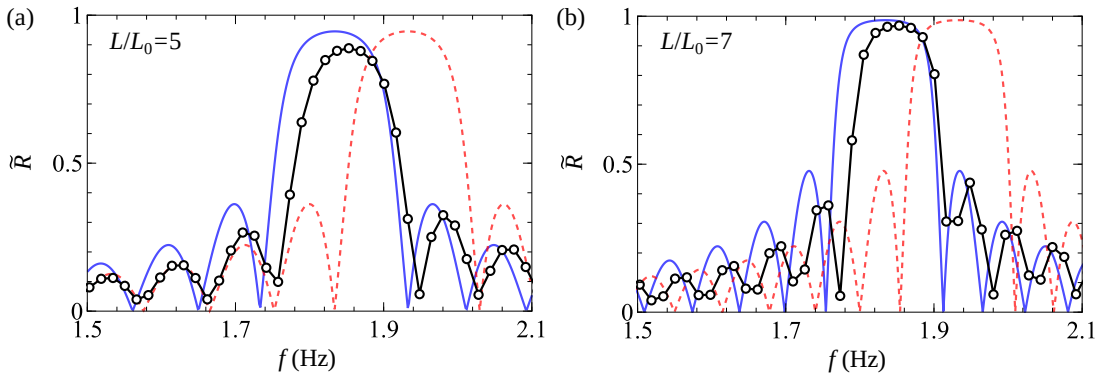

Fig. 5 Comparison of the reflection coefficient among the present solution (blue solid line, Eq.

(36)), analytical solution of Rey et al. (1996) (red dashed line, Eq. (37)), numerical solution based on the method of Seo (2014) with Scheme B (blakc dot), for varying ripple length. (a) $L/L_0 = 5$; (b) $L/L_0 = 7$.

Fig. 5 (a) and (b) depict the results of reflection coefficients under different conditions of ripple length, in which L/L_0 is fixed at 5 and 7, respectively. It is evident that the increase of ripple length can significantly enhance wave reflection of Bragg resonance, and more sub-resonances can be observed, with more peaks of reflection coefficient generated in Fig. 5 (b).

It is worth indicating that the present formula cannot predict the variation of downshift magnitude caused by the increase of L, since no terms related to the ripple length are included in it. However, the numerical solution still compares well with the present solutions, even though the ripples are sufficiently long. Thus, we assume that, for class II Bragg resonance, a limit of the wave frequency downshift exists as L tends to infinity, and the formula in Eq. (43) is the prediction for this limit. To verify this hypothesis, the resonance frequency versus the ripple length is calculated.

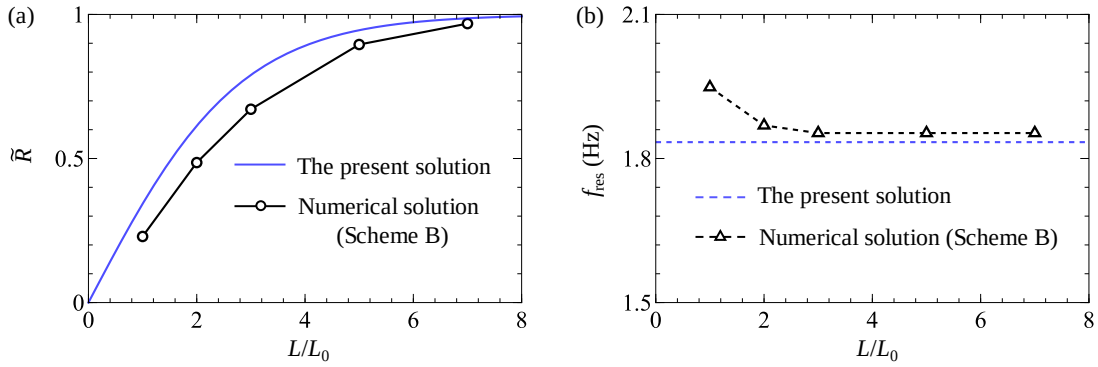

Fig. 6 Comparisons between the present solutions and numerical solutions calculated based on the method of Seo (2014) with Scheme B for (a) the reflection coefficient; (b) the resonance frequency.

In Fig. 6 (a), the reflection coefficient versus with ripple length is presented. As ripple length increases, both the present and numerical results for reflection increases up to 1, where full reflection will occur when L is sufficiently large. Furthermore, in Fig. 6 (b), the blue dashed line that corresponds to the theoretical formula in Eq. (43) does not vary with L, while the numerical solutions, symbolized by black triangle, gradually decreases with increasing ripple length and finally converges to a constant, which is approximately equal to the theoretical

prediction. Therefore, we have demonstrated the existence of the limit frequency of the class II Bragg resonance, which can be approximately predicted by the theory in Eq. (43).

Subsequently, more results are presented to further prove the generality of this observation, where different conditions of D/h are applied to calculate the results of the reflection coefficient and resonance frequency versus ripple length.

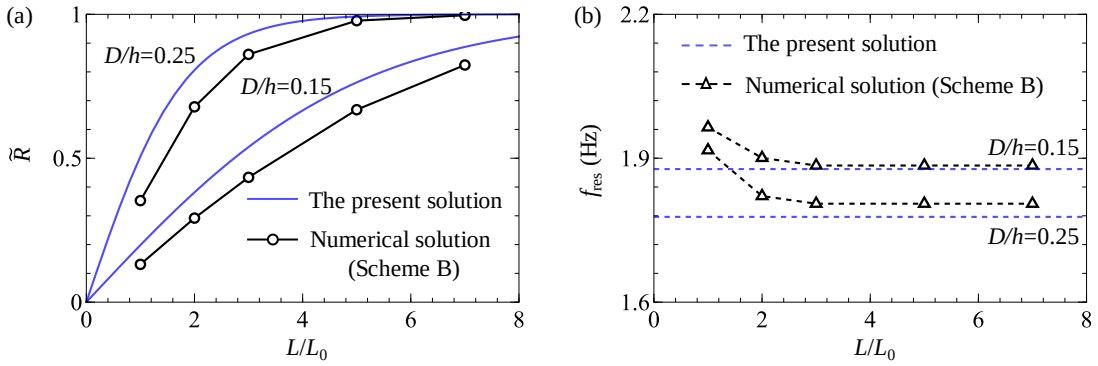

Fig. 7 (a) The reflection coefficient and (b) the resonance frequency, versus ripple length for *D/h*=0.15 and 0.25 with the present solutions and numerical solutions based on Scheme B.

In Fig. 7 (a), for both *D/h*=0.15 and 0.25, the reflection coefficient predicted by the present solution increases and converges to 1 with the increase of ripple length, with the latter arriving at full reflection earlier than the former case, achieving overall agreements with the numerical solutions despite slight overestimation. This discrepancy is probably due to evanescent modes (Guazzelli et al., 1992) that are not included in the present theoretical analysis. Moreover, as shown in Fig. 7 (b), the theoretical predictions (blue dashed line) serve as horizontal asymptotes of the resonance frequency, which restricts the resonant frequency to not exceed this sub-bound, and the frequency gradually decreases as L increases and finally converges approximately to this theoretical prediction, which further support the phenomenon observed in Fig. 6.

Notably, for the case with small ripple amplitude, *D/h*=0.15, the formula in Eq. (43) can accurately capture the resonant frequency as L tends to infinity, while for steeper ripples with *D/h*=0.25, the present theory slightly underestimates the real resonant frequency due to the third-order accuracy of the present analysis.

C. The effects of the two ripple components

In practice, the amplitudes of the two components of the ripples, D_1 and D_2, are not always equal. Therefore, it is necessary to evaluate the effects of each component and determine

which one is more effective in influencing the downshift magnitude of the resonance frequency. From the theoretical formula Eq. (43), the impacts of the two amplitudes of ripple components are different due to $\sigma_1 \neq \sigma_2$, and this formula can be rewritten as

$$f_{\text{res}}^{\text{TP}} = \tilde{f} + \frac{1 - \sqrt{1 - 4\alpha^{+}\sigma_1(D_1^2 + \chi D_2^2)}}{4\pi\alpha^{+}}, \tag{45}$$

in which χ is defined as the ratio of σ_2 to σ_1, which is expressed as a function on two dimensionless quantities, $\chi = \chi(K_2/K_1, K_1h)$, and can be used to evaluate the influence of D_1 and D_2. We restrict our discussion to $1 < K_2/K_1 < 2$ and $0 < K_1h < \infty$.

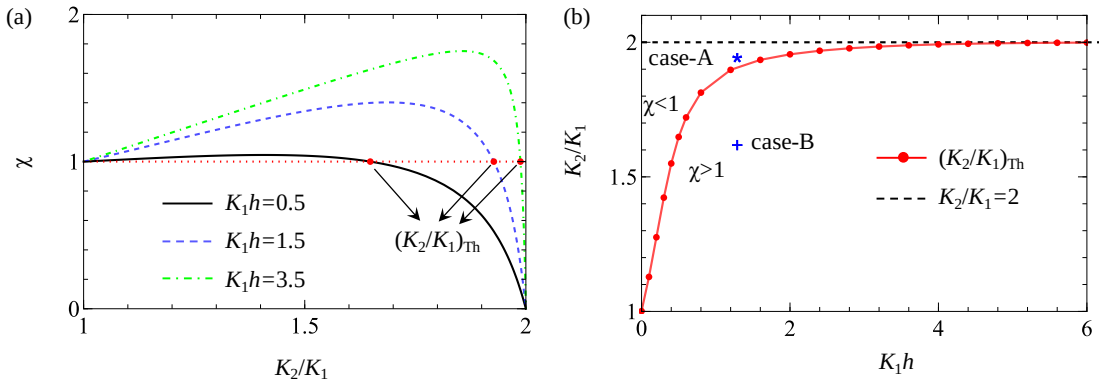

Fig. 8 (a) The function χ varying with the ratio of the two ripple wavenumbers, K_2/K_1, for different K_1h. (b) The threshold value $(K_2/K_1)_{\text{Th}}$ varying with K_1h.

Fig. 8 (a) shows the value of χ varying with K_2/K_1 for different values of K_1h, where each line has an intersection with $\chi = 1$, and the horizontal coordinate of the intersection is defined as the threshold value of the ratio of the two ripple wavenumbers, $(K_2/K_1)_{\text{Th}}$, which corresponds the condition where the effects of D_1 and D_2 on the resonance frequency are identical. When $K_2/K_1 < (K_2/K_1)_{\text{Th}}$, we have $\chi > 1$, where the amplitude of the first ripple component is more effective. Conversely, as K_2/K_1 exceeds this threshold value, the amplitude of the second component holds the primacy.

The value of $(K_2/K_1)_{\text{Th}}$ that varies with the increasing K_1h is depicted in Fig. 8 (b), in which the red line divides the domains, where $\chi < 1$ and $\chi > 1$. For a fixed K_1h, as the value of K_2/K_1 increases from 1 to 2, the downward shift of Bragg resonance will gradually transit from the first ripple component-dominant to the condition dominated by the second one. As can be seen, as K_1h tends to 0 (shallow water condition), we have $(K_2/K_1)_{\text{Th}} \to 1$. Thus, for an arbitrary K_2/K_1, the first ripple component plays a more important role in influencing the

downshift behavior. However, for deep water condition ($K_1h \to \infty$), we have $(K_2/K_1)_{\mathrm{Th}} \to 2$, where the influence of the second component is more significant for an arbitrary K_2/K_1.

To verify the hypothesis, two cases (case-A and case-B), represented by the symbols '$\star$' and '+' in Fig. 8 (b), are used to examined the effects of the two ripple components on the resonance frequency, where the water depth $h = 0.02$ m, the single ripple length $L_0 = 1.95$ m, the ripple length $L = 3.9$ m, and K_1 are fixed at $2\pi/0.0975\ \mathrm{m}^{-1}$, leading to $K_1h = 1.29$ and $(K_2/K_1)_{\mathrm{Th}} = 1.91$. The only difference between the two cases lies in the wavenumber of the second ripple component, where $K_2 = 2\pi/0.05\ \mathrm{m}^{-1}$ for case-A ($K_2/K_1 = 1.95 > (K_2/K_1)_{\mathrm{Th}}$) and $K_2 = 2\pi/0.06\ \mathrm{m}^{-1}$ for case-B ($K_2/K_1 = 1.625 < (K_2/K_1)_{\mathrm{Th}}$). The resonance frequency is calculated for varying ripple amplitudes, and three conditions are considered to examine which component is more effective in influencing the downshift,

con-(1): D_2 is fixed at $0.1h$ and D_1 is varying ($D_2/h = 0.1,\ D_1 = D$);

con-(2): D_1 is fixed at $0.1h$ and D_2 is varying ($D_1/h = 0.1,\ D_2 = D$);

con-(3): both D_1 and D_2 are varying ($D_1 = D_2 = D$).

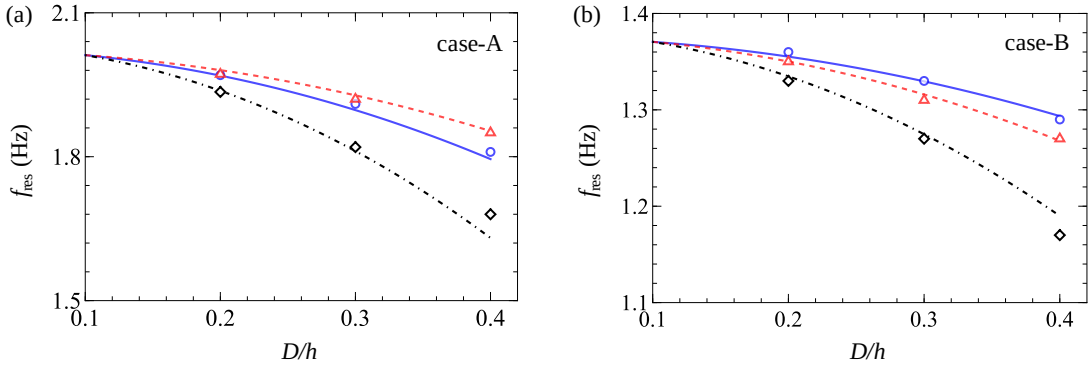

Fig. 9 Comparison of the resonance frequency predicted by the present theoretical formula (blue solid line for con-(1); red dashed line for con-(2); black dash-dotted line for con-(3), Eq. (43)) and numerical solutions (blue circle for con-(1); red triangle for con-(2); black diamond for con-(3)) based on Scheme B for varying *D/h*, (a) case-A; (b) case-B.

In Fig. 9, the comparisons between the theoretical and numerical solutions are presented for the two cases, where the solutions under con-(3) demonstrates that simultaneously increasing the magnitude of both ripple components can greatly increase the downshift magnitude. Notably, according to previous analysis, case-A corresponds to the condition where D_1 is more effective than D_2, and this prediction is supported by the results shown in Fig. 9

(a), where both theoretical and numerical solutions under con-(1) decreases more significantly than those under con-(2). Conversely, for case-B, as bottom amplitudes increase, the downshift behavior is primarily dominant by the amplitude of the second ripple component, where results (con-(2)) represented by the red line and triangle decline more significant compared to the those represented by blue line and circle.

Furthermore, the completely opposing phenomenon verifies the existence of the threshold ratio of the two ripple wavenumbers: $(K_2/K_1)_{\mathrm{Th}}$. And we have clarified the influences of each ripple component: for $K_2/K_1 < (K_2/K_1)_{\mathrm{Th}}$, the first ripple component dominates the downshift behavior, while for $K_2/K_1 > (K_2/K_1)_{\mathrm{Th}}$, the second ripple component is more effective in determining the downshift magnitude.

iv. Conclusion

In this paper, by employing the multiple-scale expansion method, we have proposed a new analytical solution for class II Bragg resonance, and based on which an exact solution that quantifies the downshift of the wave frequency of Bragg resonance is derived. Via systematic comparisons with the analytical solutions of Rey et al. (1996) and numerical solutions calculated based on the numerical method in Seo (2014), the superiority and accuracy of the present solutions in describing wave reflection and downshift magnitude are demonstrated. Moreover, the effects of ripple amplitude, ripple length and the two ripple components are studied, and there are three main conclusions.

The underlying mechanism of the downshift behavior of class II Bragg resoancne is revealed, which is induced by the interactions among wave, ripple component, conjugate ripple component, namely, the process where the wave first is reflected by a ripple component and is subsequently re-reflected by the conjugate of this ripple component, which can be represented by the wavenumbers of wave $\tilde{k}$, the first K_1 and second ripple component K_2, with $\pm(\tilde{k} + K_1 - K_1)$ and $\pm(\tilde{k} + K_2 - K_2)$.

The ripple amplitude is a primary factor governing the downshift behavior, and the increase of which can significantly intensify the downshift magnitude, and the downward trend is an approximately parabolic-shaped. In addition, the study on the effect of ripple length on class II Bragg resonance reveals that the maximum reflection increases significantly with the

increase of ripple length, where full reflection occurs as the length tends to infinity. Furthermore, as the ripple length increases, the downshift magnitude decreases and converges to a constant, which can be well captured by the newly derived formula for resonance downshift, and this phenomenon is similar to that in class I Bragg resonance (Liu, 2023; Liu et al., 2019).

The investigation on the two components of the ripple highlights that which one dominates the downward shift, and both can be the primary factor, which strongly relies on the water depth h and two two ripple wavenumbers K_1 and K_2. For a specific K_1h, a threshold ratio of the two ripple wavenumbers, $(K_2/K_1)_{\mathrm{Th}}$, exists, which is always greater than 0 and less than 2, and this threshold value indicates the identical effects of both components. As K_2/K_1 increases from 1 to 2, the first ripple component dominates the downshift behavior, when K_2/K_1 exceeds $(K_2/K_1)_{\mathrm{Th}}$, it transits to a condition dominated by the second ripple component. Notably, under shallow water condition $(K_1h \to 0)$, the threshold ratio tends to 0 $((K_2/K_1)_{\mathrm{Th}} \to 0)$, indicating that the second component is primary for arbitrary K_2/K_1. Conversely, under deep water condition $(K_1h \to \infty)$, we have threshold ratio converges to 2, where the first component is always more important for any K_2/K_1.

v. Reference

Ardhuin, F. and Herbers, T., 2002. Bragg scattering of random surface gravity waves by irregular seabed topography. Journal of Fluid Mechanics, 451: 1-33.

Ardhuin, F. and Magne, R., 2007. Scattering of surface gravity waves by bottom topography with a current. Journal of Fluid Mechanics.

Belzons, M., Rey, V. and Guazzelli, E., 1991. Subharmonic bragg resonance for surface water waves. Europhysics Letters, 16(2): 189.

Davies, A.G. and Heathershaw, A.D., 1984. Surface-wave propagation over sinusoidally varying topography. Journal of Fluid Mechanics, 144(-1): 419-443.

Fang, H., Tang, L. and Lin, P., 2023. Homotopy analysis of wave transformation over permeable seabeds and porous structures. Ocean Engineering, 274: 114087.

Friedman, B., 1956. Principles and techniques of applied mathematics, john wiley and sons. Inc., New York.

Guazzelli, E., Rey, V. and Belzons, M., 1992. Higher-order bragg reflection of gravity surface waves by periodic beds. Journal of Fluid Mechanics, 245(-1): 301.

Kirby, J.T., 1988. Current effects on resonant reflection of surface water waves by sand bars. Journal of Fluid Mechanics, 186: 501-520.

Kirby, J.T., 1993. A note on bragg scattering of surface waves by sinusoidal bars. Physics of Fluids A: Fluid dynamics, 5(2): 380-386.

Kirby, J.T. and Anton, J.P., 1990. Bragg reflection of waves by artificial bars. Coastal

Engineering Proceedings(22).

Liang, B., Ge, H., Zhang, L. and Liu, Y., 2020. Wave resonant scattering mechanism of sinusoidal seabed elucidated by mathieu instability theorem. Ocean Engineering, 218: 108238.

Liu, H.-W., 2023. An approximate law of class i bragg resonance of linear shallow-water waves excited by five types of artificial bars. Ocean Engineering, 267: 113245.

Liu, H.-w., Shi, Y.-p. and Cao, D.-q., 2015. Optimization of parabolic bars for maximum bragg resonant reflection of long waves. Journal of Hydrodynamics, 27(3): 373-382.

Liu, H.W., Li, X.F. and Lin, P.Z., 2019. Analytical study of bragg resonance by singly periodic sinusoidal ripples based on the modified mild-slope equation. Coastal Engineering, 150: 121-134.

Liu, Y. and Yue, D., 1998. On generalized bragg scattering of surface waves by bottom ripples. Journal of Fluid Mechanics, 356: 297-326.

Magne, R., Rey, V. and Ardhuin, F., 2005. Measurement of wave scattering by topography in the presence of currents. Physics of Fluids, 17(12): 126601.

Mei, C.C., 1985. Resonant reflection of surface water waves by periodic sandbars. Journal of Fluid Mechanics, 152: 315-335.

Mei, C.C., Hara, T. and Naciri, M., 1988. Note on bragg scattering of water waves by parallel bars on the seabed. Journal of Fluid Mechanics, 186(-1): 147-162.

Peng, J. et al., 2019. A laboratory study of class iii bragg resonance of gravity surface waves by periodic beds. Physics of Fluids, 31(6): 067110.

Peng, J., Tao, A.F., Fan, J., Zheng, J.H. and Liu, Y.M., 2022. On the downshift of wave frequency for bragg resonance. China Ocean Engineering(001): 036.

Rey, V., Guazzelli, É. and Mei, C.C., 1996. Resonant reflection of surface gravity waves by one‐dimensional doubly sinusoidal beds. Physics of Fluids, 8(6): 1525-1530.

Seo, S.-N., 2014. Transfer matrix of linear water wave scattering over a stepwise bottom. Coastal engineering, 88: 33-42.

Xu, D., Zhao, H., Song, Y. and Zhang, H., 2023. Steady-state waves at class ii bragg resonance. Physics of Fluids, 35(6).